

Estimation of the γ and γ' Lattice Parameters in Nickel-base Superalloys Using Neural Network Analysis

S. YOSHITAKE, V. NARAYAN, H. HARADA,¹⁾ H. K. D. H. BHADSHIA²⁾ and D. J. C. MACKAY²⁾

Department of Materials Science and Metallurgy, University of Cambridge, Pembroke Street, Cambridge CB2 3QZ, England, UK. 1) National Research Institute for Metals, Sengen, Tsukuba, Ibaraki-ken, 305-0047 Japan.

2) Mathematical and Physical Sciences Group, Darwin College, Silver Street, Cambridge CB3 9EU, England, UK.

(Received on September 9, 1997; accepted in final form on February 17, 1998)

The lattice constants of the γ and γ' phases of nickel base superalloys have been modelled using a neural network within a Bayesian framework. The analysis is based on datasets compiled from new experiments and the published literature, the parameters being expressed as a non-linear function of some eighteen variables which include the chemical composition and temperature. The analysis permits the estimation of error bars whose magnitude depends on their position in the input space. Of the many models possible, a "committee of models" is found to give the most reliable estimate. The method is demonstrated to be consistent with known metallurgical trends and has been applied towards the study of some experimental alloys.

KEY WORDS: neural networks; nickel; lattice constant.

1. Introduction

There has been considerable interest^{1,2)} in the application of nickel base superalloys for use in a multitude of industrial applications that include blades for gas turbines and jet engines. Such alloys have an impressive ability to withstand creep deformation at temperatures as high as 1000°C. The excellent properties rely on the existence of ordered Ni₃(Al, Ti) γ' precipitates which can be coherent with the disordered f.c.c structure of the γ matrix-phase. The γ' phase volume fraction can be as high as 0.6.³⁾ The γ' precipitate has a cubic structure with a cube-cube orientation with the matrix γ . The difference in the lattice parameters of the two phases is small but quite significant in at least two respects. The magnitude^{4,5)} and sign^{6,7)} of the misfit control the coarsening behavior (*e.g.* rafting⁸⁾) and indeed the way in which deformation by dislocation glide⁹⁾ is hindered at the γ/γ' interface.

There is a vast quantity of accurate lattice parameter data available in the published literature. A cursory examination of these data shows that Vegard's law, *i.e.* a linear relationship^{10,11)} between the lattice parameters and solute concentration is not valid as a method for modelling the parameters. The purpose of this work was to use instead a neural network^{12,13)} to model the changes in lattice parameter of both the γ and γ' phases as a function of their chemical composition and temperature. A neural network has the ability to model highly non-linear relationships.¹⁴⁾ Furthermore, the method permits the estimation of error bars whose magnitude depends on their position in the input space. The method shall

be described later in the text.

2. The Data Base

The database consists of lattice constants obtained from new X-ray analysis experiments and from the published literature. The compositions of the nickel base superalloys studied experimentally are shown in **Table 1**. The last five alloys in the table are commercial superalloys, whereas the others are experimental alloys developed by Harada *et al.*¹⁵⁾ using their computer models.

With the exception of CMSX4, all the alloys listed in Table 1 have identical processing and heat treatment. They were directionally solidified and then homogenised for four hours at 1300°C, followed by air cooling to 980°C where they were annealed for five hours. They were then cooled to 850°C and held there for sixteen hours. The alloy CMSX4 however, was aged for five and sixteen hours at temperatures 1120 and 870°C respectively. These heat treatments are well established to produce fine cuboidal γ' precipitates in the γ matrix with volume fractions that exceed 0.6. The alloy samples were filed to powder with approximate particle size of 60 mm for the purpose of X-ray analysis. This particle size mitigates the effects of any oxidation at higher temperatures. Prior to X-ray analysis, the powder samples were annealed at 900°C for 20 min to remove any mechanical strain produced during filing.

The X-ray equipment consisted of a Rigaku Rotorflex RU-200 BV diffractometer with a Cu rotating anode and a high temperature vacuum specimen chamber. The anode operated at 55 kV and 180 mA at high tempera-

Table 1. The chemical compositions for alloys examined by high temperature X-ray diffraction.

| Alloy | Composition (at%) bal Ni | | | | | | | | | |
|---------|--------------------------|-------|------|------|-------|------|------|------|------|------|
| | Co | Cr | Mo | W | Al | Ti | Nb | Ta | Hf | Re |
| TMS-1 | 8.12 | 6.75 | 0.0 | 5.76 | 12.30 | 0.0 | 0.0 | 1.83 | 1.83 | 0.0 |
| TMS-6 | 0.0 | 9.98 | 0.0 | 2.99 | 11.58 | 0.0 | 0.0 | 3.59 | 3.59 | 0.0 |
| TMS-12 | 0.0 | 7.20 | 0.0 | 4.45 | 11.29 | 0.0 | 0.0 | 2.67 | 2.67 | 0.0 |
| TMS-17 | 0.0 | 7.34 | 0.0 | 3.53 | 11.79 | 0.0 | 0.0 | 3.87 | 3.87 | 0.0 |
| TMS-19 | 0.0 | 7.47 | 0.0 | 2.80 | 11.09 | 0.0 | 0.0 | 4.47 | 4.47 | 0.0 |
| TMS-26 | 8.82 | 6.34 | 1.26 | 3.97 | 11.98 | 0.0 | 0.0 | 2.84 | 2.84 | 0.0 |
| TMS-30 | 8.36 | 6.68 | 0.0 | 3.54 | 12.17 | 0.0 | 0.0 | 2.65 | 2.65 | 0.85 |
| TMS-61 | 0.0 | 12.35 | 3.47 | 0.0 | 10.44 | 2.47 | 1.15 | 0.28 | 0.28 | 0.0 |
| TMS-62 | 0.0 | 8.54 | 4.04 | 0.0 | 12.08 | 1.06 | 1.45 | 0.0 | 0.0 | 0.0 |
| TMS-63 | 0.0 | 7.80 | 4.60 | 0.0 | 12.80 | 0.0 | 0.0 | 2.80 | 2.80 | 0.0 |
| TMS-67 | 0.0 | 5.84 | 5.42 | 0.0 | 13.21 | 0.0 | 0.0 | 1.87 | 1.87 | 0.0 |
| TMS-70 | 6.54 | 6.27 | 4.64 | 0.0 | 12.97 | 0.0 | 0.0 | 2.79 | 2.79 | 0.0 |
| NSR100 | 0.0 | 9.77 | 0.62 | 3.28 | 11.96 | 1.50 | 0.0 | 1.09 | 1.09 | 0.0 |
| CMSX4 | 9.80 | 7.60 | 0.38 | 2.12 | 12.60 | 1.27 | 0.0 | 2.18 | 2.18 | 0.98 |
| RR2000* | 13.77 | 10.56 | 1.70 | 0.0 | 11.01 | 4.60 | 0.0 | 0.0 | 0.0 | 0.0 |
| SRR99 | 5.0 | 9.63 | 0.0 | 3.04 | 12.00 | 2.70 | 0.0 | 0.91 | 0.91 | 0.0 |
| MC2 | 5.10 | 9.30 | 1.30 | 2.06 | 11.20 | 2.50 | 0.0 | 2.00 | 2.00 | 0.0 |

NSR100 abbreviation for NASAIR100. *RR2000 contains small amounts of vanadium.

Table 2. The number of lines of data used in the neural network analysis.

| | γ phase | γ' phase |
|-----------------|----------------|-----------------|
| Measured by XRD | 133 | 133 |
| Databook | 321 | 177 |
| Total | 454 | 310 |

Table 3a. The variables used in the neural network analysis for the γ phase. The information is mostly presented to two decimal places.

| Variables | Range | Mean | Standard deviation |
|----------------------|---------------|--------|--------------------|
| Temperature (°C) | 15–1 100 | 316 | 344 |
| Nickel (at%) | 31.1–100.00 | 79.32 | 15.30 |
| Cobalt (at%) | 0–68.90 | 2.98 | 7.82 |
| Chromium (at%) | 0–34.80 | 7.74 | 9.55 |
| Molybdenum (at%) | 0–26.51 | 2.38 | 5.13 |
| Tungsten (at%) | 0–15.50 | 1.26 | 2.40 |
| Aluminium (at%) | 0–17.00 | 2.02 | 2.85 |
| Titanium (at%) | 0–9.50 | 0.19 | 0.87 |
| Niobium (at%) | 0–7.90 | 0.63 | 0.52 |
| Tantalum (at%) | 0–8.02 | 0.29 | 0.72 |
| Hafnium (at%) | 0–1.12 | 0.00 | 0.06 |
| Rhenium (at%) | 0–2.67 | 0.07 | 0.39 |
| Vanadium (at%) | 0–4 192 | 1.41 | 6.33 |
| Iron (at%) | 0–35.00 | 1.60 | 5.28 |
| Gallium (at%) | 0–15.72 | 0.20 | 1.45 |
| Copper (at%) | 0–32.41 | 0.38 | 2.61 |
| Gold (at%) | 0–6.7 | 0.10 | 0.50 |
| Lattice constant (Å) | 3.5166–3.6606 | 3.5730 | 0.0410 |

tures. The heating mechanism consisted of a thermocouple, aluminium stage wrapped in platinum heater coil and a platinum sample holder connected to a second thermocouple. The specimen alloy powder was embedded on standard α -alumina powder to avoid chemical reaction with the platinum holder and the stage was covered with three layers of nickel foil to reduce thermal emissions.

The X-ray measurements were made at room tem-

Table 3b. The variables used in the neural network analysis for the γ' phase. The information is mostly presented to two decimal places.

| Variables | Range | Mean | Standard deviation |
|----------------------|------------------|--------|--------------------|
| Temperature (°C) | 20–1 100 | 357 | 387 |
| Nickel (at%) | 32–90.20 | 72.82 | 4.81 |
| Cobalt (at%) | 0–25.00 | 1.24 | 2.71 |
| Chromium (at%) | 0–34.80 | 3.01 | 5.38 |
| Molybdenum (at%) | 0–4.82 | 0.64 | 1.18 |
| Tungsten (at%) | 0–4.87 | 0.96 | 1.36 |
| Aluminium (at%) | 0–26.00 | 15.01 | 6.82 |
| Titanium (at%) | 0–20.00 | 1.25 | 2.74 |
| Niobium (at%) | 0–8.03 | 0.18 | 0.79 |
| Tantalum (at%) | 0–10.14 | 1.74 | 2.10 |
| Hafnium (at%) | 0–4.04 | 0.04 | 0.31 |
| Rhenium (at%) | 0–0.25 | 0.01 | 0.04 |
| Vanadium (at%) | 0–10.00 | 0.14 | 0.98 |
| Iron (at%) | 0–64.00 | 1.08 | 6.27 |
| Gallium (at%) | 0–29.80 | 1.86 | 6.13 |
| Lattice constant (Å) | 3.52273–3.641508 | 3.5950 | 0.27 |

perature, 300, 500, 600, 700, 800, 900, 1 000 and 1 100°C. The (200) and (311) peaks for the γ and γ' phases were measured in steps of 0.01° 2 sec. Prior to each scan the sample was allowed to stabilise its temperature for approximately 15 min. The signals were measured twice and added together to produce a single profile with enhanced the signal-to-noise ratio. The X-ray profile consisted of overlapping γ and γ' peaks which were deconvoluted using the profile fitting program PROFIT¹⁶⁾ that employs a split Pearson VII function. The use of the latter function enables the detailed analysis of peak asymmetry and thus allows the separation of the γ and γ' signals and the broadening of peaks. The compositions of the γ and γ' phases at high temperatures were calculated using the alloy design program developed by Harada.¹⁵⁾

A significant proportion of the lattice parameters that compose the database were obtained from Pearson's

datobook¹⁷⁾ and Ochiai *et al.*^{18,19)} The size of the data base is important to evaluate the plausibility of the predictions. In **Table 2** we have summarized the number of measured and reported lattice parameters. The lattice constants of the γ and γ' phases in the nickel base superalloys were measured in a mixed two-phase microstructure. The published lattice parameter data are for single phase samples. It is possible that coherency strain in the mixed microstructure can introduce an error of 0.01–0.1 % in the measurements, as shown by Ohno *et al.*²⁰⁾ Such an error would be reflected in the model perceived level of noise in the dataset. We construct a separate database for the γ and γ' phases respectively. The range, mean and standard deviation of the variables in the databases are listed in **Table 3**.

3. The Neural Network Model

The temperatures and alloy compositions were used as inputs and the lattice constant was the output of the neural network model. We have a separate database of inputs and output for the γ and γ' phases respectively. The inputs and output were first normalised within the range ± 0.5 :

$$x_N = \frac{x - x_{\min}}{x_{\max} - x_{\min}} - 0.5 \dots\dots\dots (1)$$

where x_N is the normalised value of x , x_{\max} is the maximum value and x_{\min} is the minimum value of each variable. This normalisation allows convenient comparison of the relative importance of individual inputs on the output.

The structure of the neural network model used is shown schematically in **Fig. 1**. The inputs and outputs as shown are connected through hidden units where the inputs x_j are operated by a hyperbolic tangent transfer function to obtain the hidden units h_i defined as:

$$h_i = \tanh\left(\sum_j w_{ij}^{(1)} x_j + \theta_i^{(1)}\right) \dots\dots\dots (2)$$

where $\theta_i^{(1)}$ is defined as the bias that is analogous to the constant that appears in the linear regression technique, $w_{i,j}$ are defined as the weights that determine the strength of the transfer function. The output is obtained as follows:

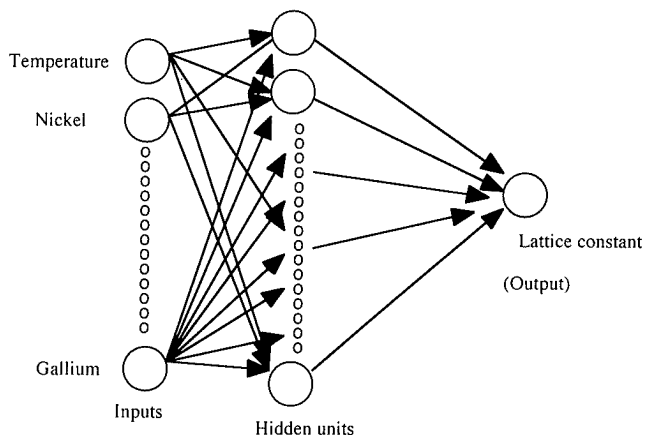


Fig. 1. The neural network structure.

$$y = \sum_i w_i^{(2)} h_i + \theta^{(2)} \dots\dots\dots (3)$$

where $w_i^{(2)}$ and $\theta^{(2)}$ are a new set of weights and a bias. Equations (2) and (3) define the neural network structure that connects the inputs to the output. The weights and biases however, are unknowns to be determined through “training” using the Bayesian back propagation scheme, which involves a minimisation of the function:

$$M(w) = \beta E_D + \sum_c \alpha_c E_{w(c)} \dots\dots\dots (4)$$

where E_D is defined as:

$$E_D(w) = \frac{1}{2} \sum_m \sum_i (y_i(x^m, w) - t^m)^2 \dots\dots\dots (5)$$

where the data set $\{x^m, t^m\}$ consists of x^m inputs related to a particular target t^m (m is a label of the pairs). The aim is to determine a set of weights in a manner that minimises E_D but without overfitting to noise. Thus, the regularisers E_w are included so that smooth solutions of $y(x^m, w)$ are favoured and the possibility of fitting to noise in the experimental data can be reduced. The simplest regulariser has the form $E_w = (1/2) \sum w_i^2$. We shall use however, the more sophisticated automatic relevance determination model²¹⁾ as described in the literature.

The number of hidden units used determines the complexity of the neural network and more accurate

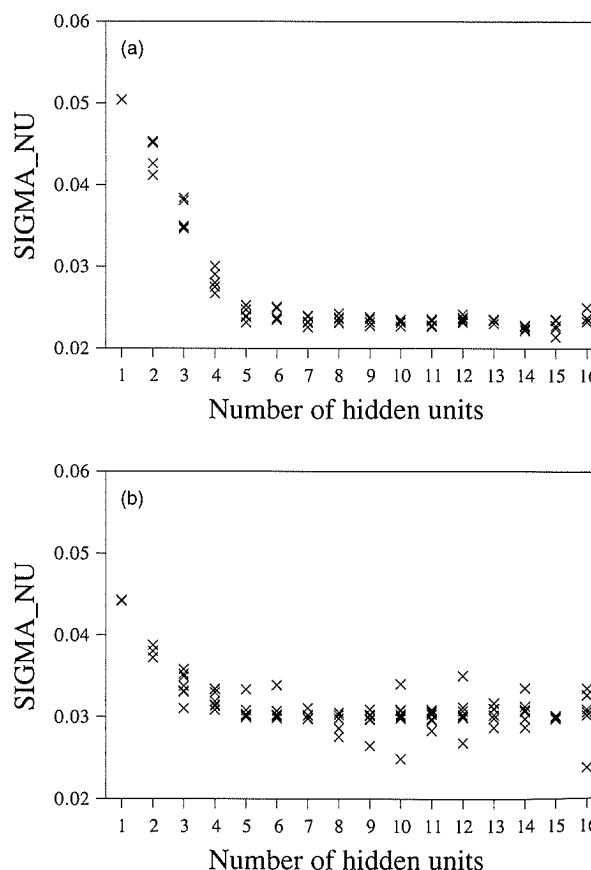


Fig. 2. The variation in σ_v for the lattice parameters of (a) γ and (b) γ' phases respectively as a function of hidden units.

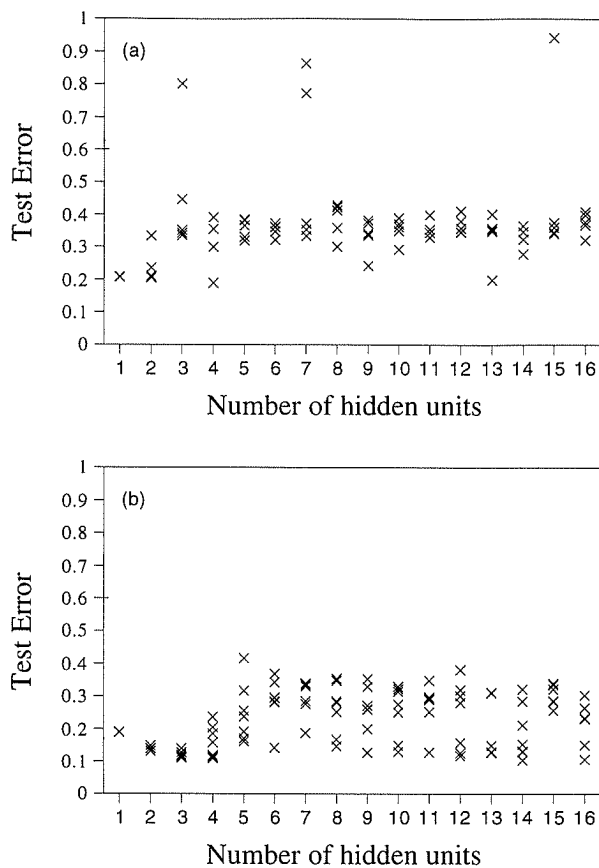


Fig. 3. The test error for the lattice parameters of (a) γ and (b) γ' phases respectively as a function of hidden units.

predictions occur with increased number of hidden units. The value of σ_v decreases monotonically with the number of hidden units for both the γ and γ' phases (Fig. 2). The test error, defined as the value of the error function for unseen data is shown for both the γ and γ' phases in Fig. 3. The best model may be defined as that with the smallest test error. This would be appropriate, for situation where only scalar prediction (*i.e.* no error bars) are required. MacKay has shown, when making predictions with error bars, the best model should be decided according to a quantity the “log predicted error”. Using the log predicted error, unlike the test error, wild predictions are penalised less if they have large error bars. When using noisy data, common in many experimental situation, some wild predictions must be expected.

4. The Committee Model

It is often the case with noisy data that models with different complexity make different predictions. In these circumstances, the prediction made by a committee of models may be more reliable than using a single model. Figures 2 and 3 describe a population of models that can be ranked according to the magnitude of the test error. We start a committee by using N models ranked by the “log predicted error”. The committee is formed through combining the best N models (where $N=1, 2, 3, \dots$) such that the mean prediction of the committee is:

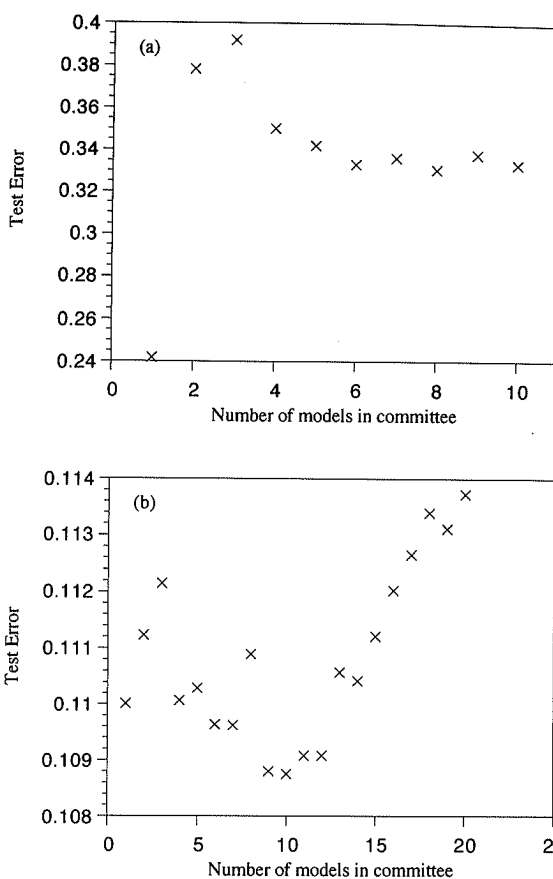


Fig. 4. The change in the test error with the number of models used in the committee for (a) the γ and (b) γ' phases respectively.

$$\bar{y} = \frac{1}{N} \sum_{i=1}^N y_i \dots\dots\dots(6)$$

with associated error in \bar{y} expressed as:

$$\sigma^2 = \frac{1}{N} \sum_{i=1}^N \sigma_i^2 + \frac{1}{N} \sum_{i=1}^N (y_i - \bar{y})^2 \dots\dots\dots(7)$$

Figure 4 shows the changes in the test error with the number of models used to form a committee. The figure shows that a ten model committee is favourable for the γ' phase, whereas for the γ phase the use of a single model is appropriate. Committee predictions are compared against experimental data in Fig. 5. The behaviour of the committee model consisting of individual models retrained on the entire dataset is illustrated in Fig. 6. The inputs to output mapping becomes more accurate, after retraining. The purpose of the division into training and test data was to identify models with the optimal level of complexity. Once that is done, its quite reasonable to use the entire dataset for retraining, but without changing the complexity of the model. Since the committee complexity is not changed after retraining, its ability to generalise is not significantly effected.

5. The Significance of Individual Inputs on the Lattice Constant

The metallurgical significance of the inputs is now considered. Figures 7 and 8 illustrate the significance of

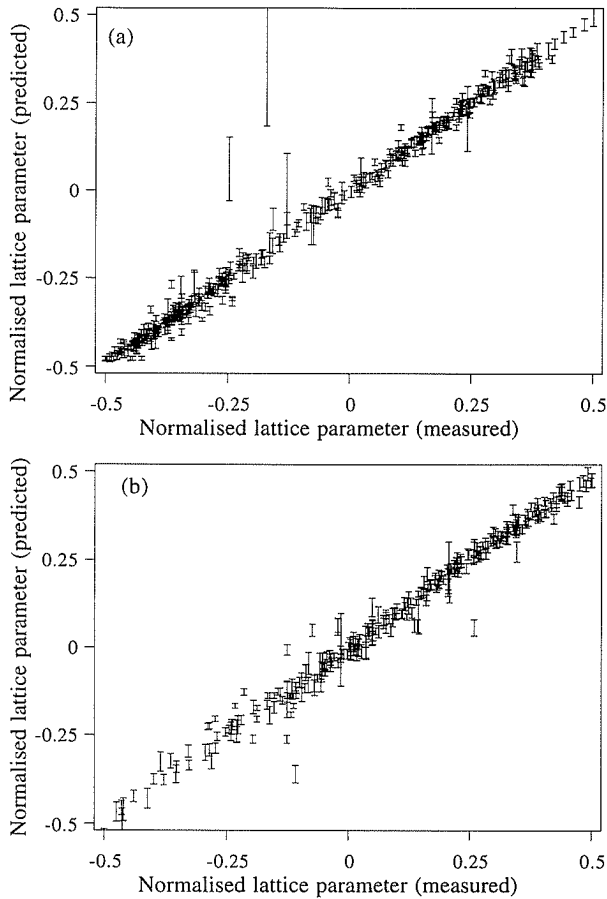


Fig. 5. The comparison of the measured lattice parameter the (a) γ and (b) γ' phases with the neural network committee prediction, using the test data.

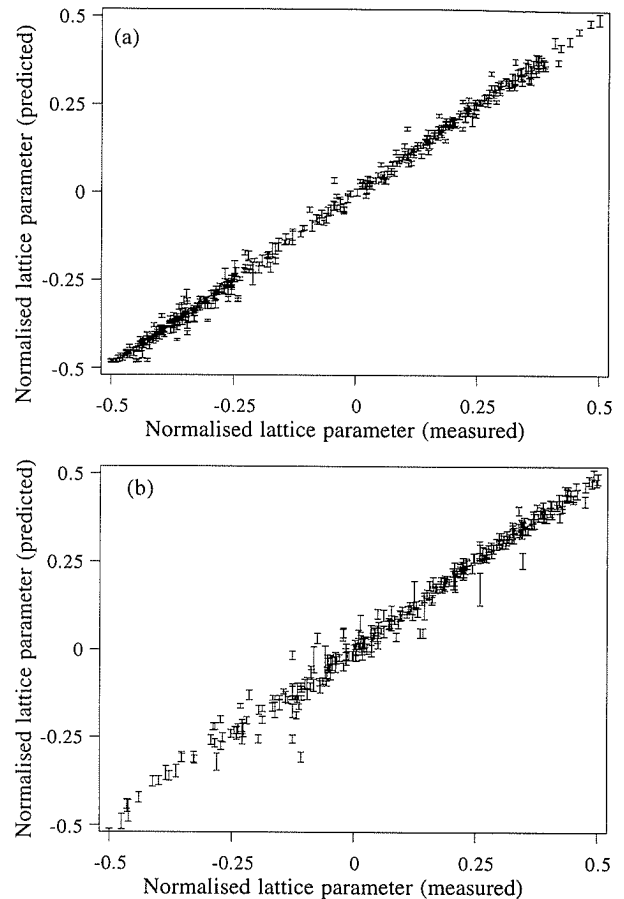


Fig. 6. The comparison of the normalized lattice parameter measured of (a) γ and (b) γ' phases with the neural network committee prediction after retraining on all the data.

each of the inputs for the γ and γ' phases, as perceived by the neural network model, in effecting the lattice constants within the limitations of the dataset. For some inputs we observe a significant scatter of σ_w (for γ' phase model) for each member of the committee, indicating that the relationship identified for that input has a high uncertainty. However clear trends are observed. A large value of σ_w implies that the input concerned explains a relatively large amount of the variation in the lattice constant in the dataset (analogous to the partial correlation coefficient used in the multiple regression analysis approach). The σ_w value is not an indication of the sensitivity of the lattice constant to a particular input. The interpretation of σ_w is best understood by the predictions made in the following section. The results show variation in lattice constant expected from cluster variation calculations.²⁾

6. Application of the Model

We chose to predict the lattice constants of the γ and γ' phase for three typical nickel-base superalloys: (i) TMS63 which has a large negative lattice misfit at all temperature and thus shows the most superior creep rupture lifetime (ii) TMS19 that has a large positive lattice misfit and thus poor creep rupture lifetime (iii) CMSX4 a commercial single crystal superalloy that has a complex

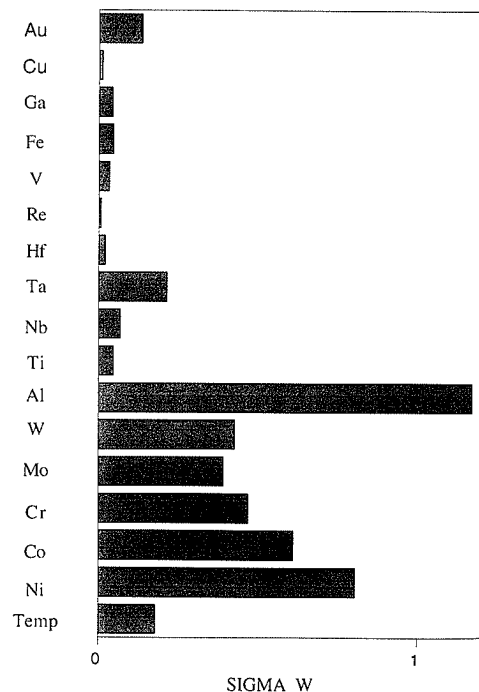


Fig. 7. The bar chart of the model perceived significance for each input used in the 9 hidden units single neural network model for the γ phase (the seed of the random number used to start the training was 30).

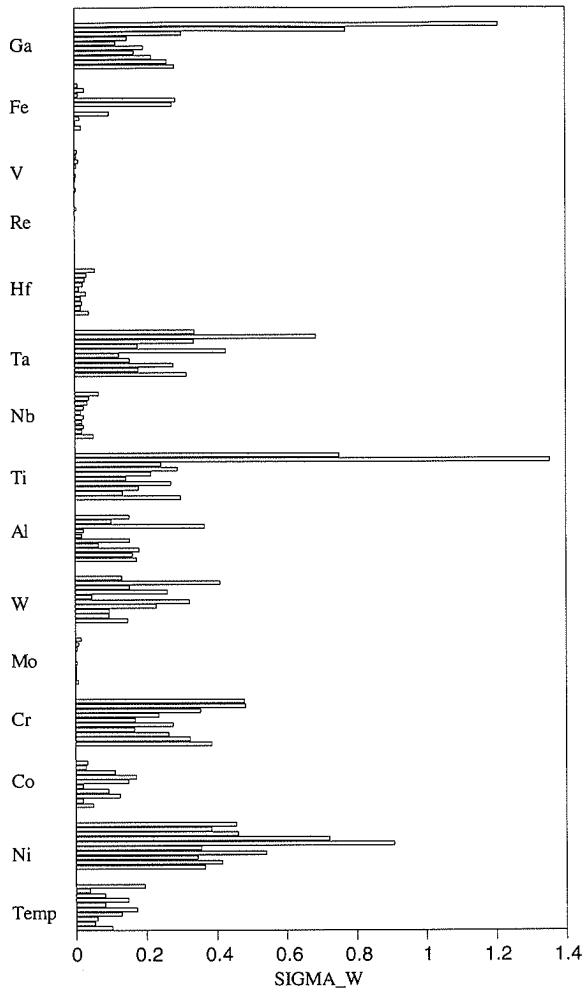


Fig. 8. The bar chart of the model perceived significance for each input used in the ten model “committee” to predict the lattice parameter of the γ' phase. For each weight the bars (top to bottom) correspond to hidden units 14, 16, 4, 3, 3, 4, 3, 4, 3 and 3 were the seed of random number used to start the training was 50, 10, 20, 1, 10, 40, 30, 30, 60 and 30 respectively.

composition that includes rhenium. In **Fig. 9** we present the predictions for these alloys in the γ phase. The predictions have very small error bars and are in the range of the experimental measurements. **Figure 10** contains the prediction for the alloys CMSX4, TMS19 and TMS63 for the γ' phase, these predictions also compare favourably with the X-ray measurements.

We shall next focus on alloy TMS63 that has been reported to have the best creep rupture time and study the variation of the lattice constant with most of the individual alloying elements. In this study, a single element in TMS63 was chosen and its concentration was changed. The predictions are at the commercially critical temperature of 900°C and are shown in **Figs. 11** and **12** for the γ phase. The chemical compositions of the γ and γ' phases of alloy TMS63 at 900°C are shown in **Table 4**. The results illustrate that raising the concentration of most variables increases the γ phase lattice constant (with elements Al, Nb and Mo being particularly effective). It is emphasised here that the results are plotted as a function of the γ and γ' phase compositions rather than alloy composition. The partitioning of elements

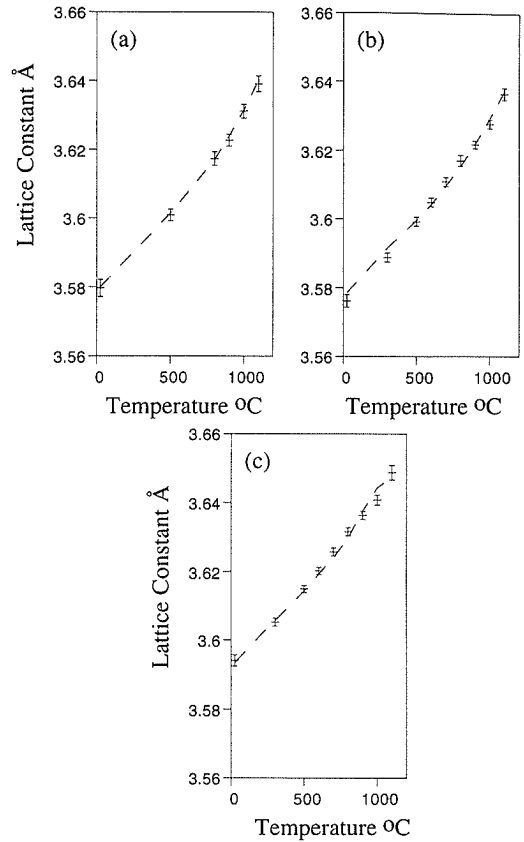


Fig. 9. The lattice constant predicted for alloy (a) CMSX4 (b) TMS19 and TMS63 for the γ phase compared with the measured value (dotted line).

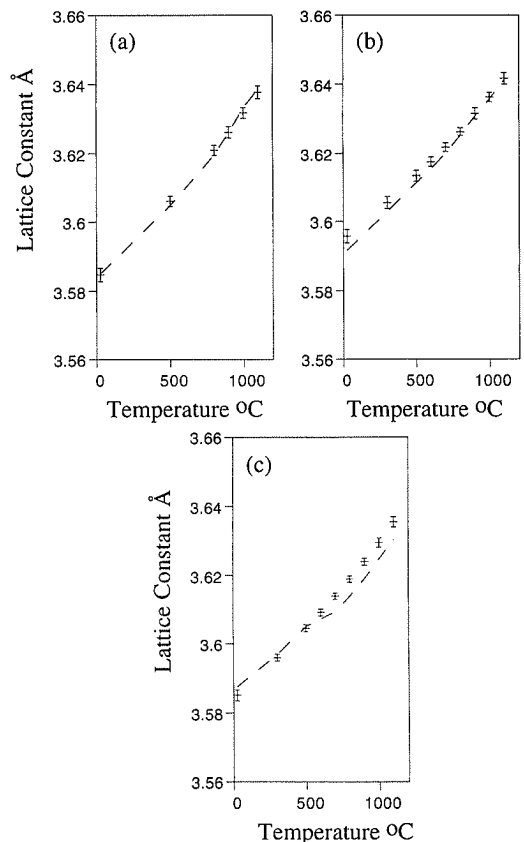


Fig. 10. The lattice constant predictions for alloy (a) CMSX4 (b) TMS19 and TMS63 for the γ' phase.

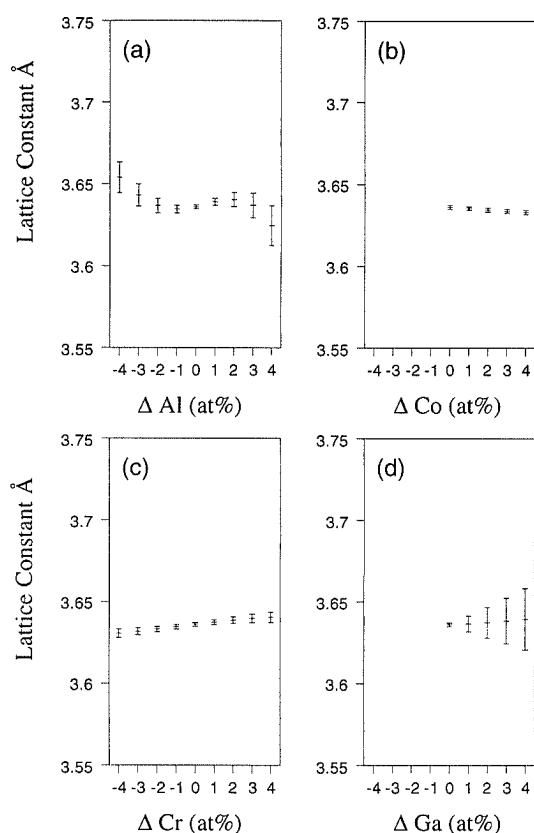


Fig. 11. The deviation of lattice constant with variation in (a) Al (b) Co (c) Cr and (d) Ga compositions (at%) from γ phase TMS63 at the temperature of 900°C.

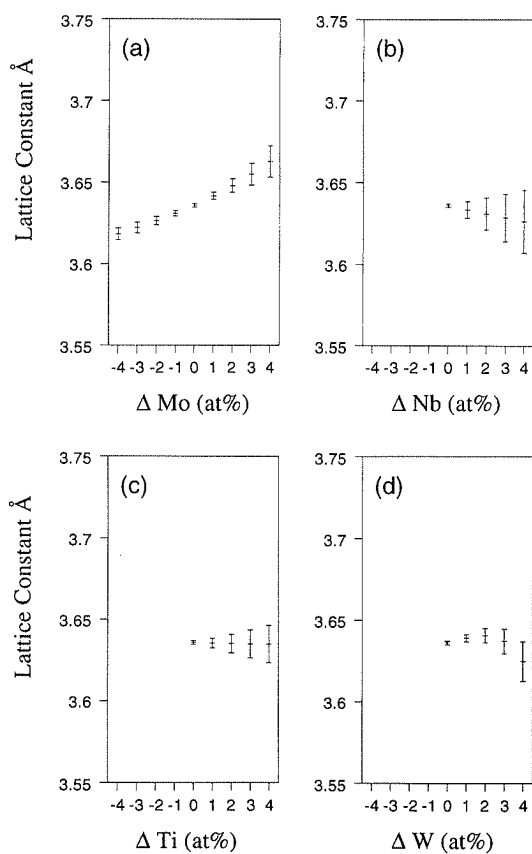


Fig. 12. The deviation of lattice constant with variation in (a) Mo (b) Nb (c) Ti and (d) W compositions (at%) from γ phase TMS63 at the temperature of 900°C.

Table 4. The chemical compositions of the γ and γ' phases of alloy TMS63 at 900°C.

| Phase | The composition of TMS63 (at%) bal Ni at 900°C | | | | | | | | |
|-----------|------------------------------------------------|-----|------|------|-----|------|-----|-----|------|
| | Ni | Co | Cr | Mo | W | Al | Ti | Nb | Ta |
| γ | 68.9 | 0.0 | 17.0 | 9.25 | 0.0 | 4.05 | 0.0 | 0.0 | 0.82 |
| γ' | 73.6 | 0.0 | 3.35 | 2.35 | 0.0 | 17.0 | 0.0 | 0.0 | 3.7 |

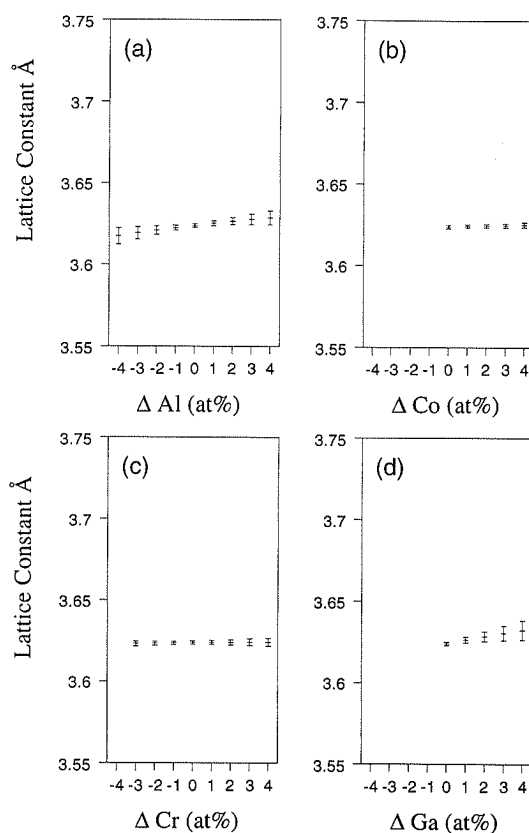


Fig. 13. The deviation of lattice constant with variation in (a) Al (b) Co (c) Cr and (d) Ga compositions (at%) from γ' phase TMS63 at the temperature of 900°C.

between the γ and γ' is a separate issue not treated in this paper. The predictions for the γ' phase are shown in Figs. 13 and 14. We note, that the γ' phase lattice constant is not that sensitive to element changes as is the γ phase. We have only examined the variation of the lattice constant with one element at a time, though the method permits variation in any number of elements.

7. Conclusions

We have constructed a neural network model within a Bayesian framework to predict the temperature dependent lattice constant of the γ and γ' phases of nickel superalloys. The neural network employs a committee of models which is more reliable than using a single model. In addition, the error bars of the committee predictions are expected to be more reliable. Reasonable predictions have been made for several alloys which agree with X-ray measurements. The variation of the lattice constant with the concentration of individual alloying elements and with temperature can now be embodied

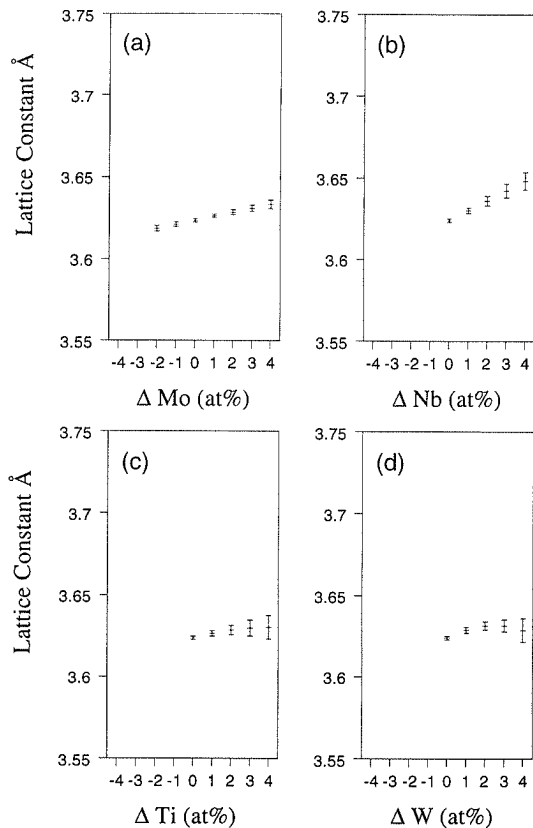


Fig. 14. The deviation of lattice constant with variation in (a) Mo (b) Nb (c) Ti and (d) W compositions (at%) from γ' phase TMS63 at the temperature of 900°C.

into other computer programs which deal with the partitioning of solutes between the γ and γ' phases.

It has been demonstrated that the neural network technique can reveal information in cases where (i) experiments cannot be designed to study each variable in isolation and (ii) the theoretical modelling of the physical system is difficult due to its complexity. The neural network scheme has the advantage that the network summarise information in an empirical manner

and may be retrained once new data are made available to obtain more accurate predictions.

Acknowledgements

V. Narayan would like to thank Catherine Neal for useful discussion, Naomi Chester for computational support and the EPSRC for funding the project.

REFERENCES

- 1) J. M. Sanchez, J. R. Barefoot, R. N. Jarrett and J. K. Tien: *Acta Metall.*, **32** (1984), 1519.
- 2) M. Enomoto and H. Harada: *Metall. Trans. A*, **20** (1989), 649.
- 3) R. W. Guard and J. H. Westbrook: *Trans. Metall. AIME*, **215** (1959), 807.
- 4) D. A. Grose and G. S. Ansell: *Metall. Trans. A*, **12** (1981), 1631.
- 5) R. C. Ecob, R. A. Ricks and A. J. Porter: *Scr. Metall.*, **16** (1982), 1085.
- 6) A. Fedholm and J. L. Strudel: *Superalloys*, (1984), 211.
- 7) D. F. Lahrman, R. D. Field, R. Darolia and H. L. Fraser: *Acta Metall.*, **36** (1988), 1309.
- 8) J. K. Tien and S. M. Copley: *Metall. Trans.*, **2** (1971), 215.
- 9) A. Pineau: *Acta Metall.*, **24** (1976), 559.
- 10) H. Harada, M. Yamazaki, Y. Koizumi, N. Sakuma and N. Furuya: Conf. Proc. D. High Temperature Alloys for Gas Turbines, Reidel Publishing Company, Boston, MA, (1982).
- 11) H. Harada, K. Ohno, T. Yamagata, T. Yokokawa and M. Yamazaki: 6th Int. Symp. Superalloys, Seven Springs, USA, Sept. (1988), 18.
- 12) D. J. C. MacKay: *Neural Computation*, **4** (1992), 415.
- 13) D. J. C. MacKay: *Neural Computation*, **4** (1992), 448.
- 14) D. J. C. MacKay: *Neural Computation*, **4** (1992), 698.
- 15) H. Harada, T. Yamagata, S. Nakazawa, K. Ohno and M. Yamazaki: Proc. of Conf. High Temperature Materials for Power Engineering, Liege, Belgium, (1990), 1319.
- 16) H. Toraya: *J. Appl. Crystallogr.*, **21** (1988), 192.
- 17) W. B. Pearson: A handbook of lattice spacing and structures of metals and alloys, Pergamon Press, Oxford, 1-2 (1958).
- 18) S. Ochiai, S. Oyama and T. Suzuki: *Acta Metall.*, **32** (1984), 289.
- 19) S. Ochiai, Y. Mishima and T. Suzuki: *Bull. PME (TIT)*, **15** (1984), 53.
- 20) K. Ohno, K. Ohsumi, H. Harada, T. Yamagata and M. Yamazaki: *Adv. X-ray Anal.*, **34** (1991), 493.
- 21) D. J. C. MacKay: *Networks. Computation in Neural Systems*, **6** (1995), 469.